Appendix to Chapter 3

Examples of super-resolution imaging with smFPs: Multiple authors have contributed to these experiments. I have included this to give an idea of the capacity of smFPs to perform as high resolution imaging tools and thereby facilitate multi – color super-resolution imaging.

5.1 Array tomography

Array tomography (AT) is a sample preparation and imaging method that enables large-volume imaging of fluorescent signals at higher resolution than confocal fluorescence microscopy (Micheva and Smith 2007). Compared to the optical sections generated by confocal or two-photon microscopy, which typically generate planes with > 700 nm z-axis resolution, AT relies on the physical sectioning of plasticized samples into ultra-thin, planarized arrays amenable to wide-field imaging. Physical sectioning improves the Z-axis resolution roughly 10-fold, while the lateral X-Y resolution remains diffraction-limited as in other conventional fluorescence imaging approaches. However, the heavy fixation, dehydration and subsequent resin embedding of tissue samples limits adequate antibody labeling to a small set of highly expressed proteins whose antigenicity is preserved throughout the sample preparation (Micheva and Smith 2007). smFPs, being more antigenic than conventional epitopes, should allow for the staining and imaging of a broader range of molecular targets using AT.

To establish the utility of smFPs for AT, we chose to examine synaptic connectivity between hippocampal CA1 pyramidal cells and genetically identified CA1 interneurons. *Sst*-IRES-Cre mice (Lovett-Barron, Turi et al. 2012), in which the Cre

recombinase coding sequence has been knocked into the endogenous somatostatin (*Sst*) locus, were bred with the *Thy-1*:eGFP mouse line M (Feng, Mellor et al. 2000), and AAV virus expressing either FLEX-*CAG*-smFP_FLAG or FLEX-*CAG*-tdTomato constructs were injected into dorsal hippocampus of heterozygous mice (**Methods**). To demonstrate the advantage of smFP labels/probes over existing labels, we visualized the synaptic connectivity of *somatostatin*-positive interneurons (expressing either smFP_FLAG or tdTomato, for comparison) onto the dendrites of GFP-expressing CA1 pyramidal cells; antibodies against the endogenous protein synapsin labeled functional synapses.

Anti-FLAG immunolabeling of *Sst*-Cre neurons expressing smFP_FLAG constructs enabled visualization of the entire somato-dendritic axis of *somatostatin*-Cre neurons, including small-diameter axonal fibers in the *stratum lacunosum moleculare* (SLM) located up to 500 μm from the cell soma. smFP_FLAG-labeled axons in the SLM exhibited varicosities but not blebs (**Supp. Fig. 8)** and were found to form putative pre-synaptic (synapsin[+]) terminals onto the distal dendrites of GFP^{+} pyramidal cells in serial ultra-thin sections (**Fig. 5b**), suggesting the smFP_FLAG epitope yielded a complete fill without any obvious toxicity or disruption of synaptic connectivity. Additional arrays demonstrated that both monoclonal and polyclonal anti-FLAG antibodies worked exceptionally well with secondary antibodies conjugated to several commonly used fluorophores, including more difficult (*i.e.* existing dyes are dim and photolabile) imaging channels such as 405 nm (**Supp. Fig. 8b**). The bright smFP fluorescence yielded high signal-to-noise wide-field images in as little as 80 msec/field, dramatically reducing the imaging time required for collection of large AT volumes.

In animals expressing tdTomato in SST positive interneurons, the native tdTomato signal progressively decreased between ultrathin sectioning and subsequent imaging. During imaging, wide-field exposure times of up to 5 seconds (*i.e.* two orders of magnitude longer) were required to adequately visualize distal tdTomato axonal processes in ultrathin sections (data not shown). Attempts to recover the tdTomato signal with either commercial or in-house anti-RFP antibodies resulted in images with higher background levels and generally poorer quality, rendering it nearly impossible to trace even relatively large-diameter axons across sections. In samples requiring longer exposures, bleed-through of the tdTomato signal into the green channel also became apparent due to the broad excitation and emission spectra of this FP. Thus, the smFP toolkit has advantages over existing FP reagents in connectomics experiments that call for labeling multiple genetically defined neuronal populations. smFPs facilitate amplification in cases where endogenous FP fluorescence is significantly reduced during sample preparation and/or when anti-FP antibodies result in increased background fluorescence.

5.2 Super-resolution STORM imaging

Stochastic optical reconstruction microscopy (STORM) is a wide-field super-resolution fluorescence imaging approach that overcomes the diffraction limit in the lateral and axial dimensions *via* stochastic activation of individual photoswitchable molecules and precise localization of the activated molecules (Rust, Bates et al. 2006, Huang, Wang et al. 2008). Individual photoswitchable fluorophores are sequentially activated and imaged; the diffraction-limited images (point-spread functions) of

individual emitters are then fit to determine their centroid positions with a precision dependent on the number of photons collected. Replotting the centroid positions of each individual molecule allows for the reconstruction of a super-resolution image. To achieve sufficient localization density to satisfy the Nyquist sampling criterion for image reconstruction, probe density is of paramount importance. In addition to providing tags for proteins for which there are no useful antibodies, smFPs could benefit super-resolution imaging by increasing the density of probe localizations through the large number of antibody-binding sites on each individual smFP.

To examine the efficacy of smFPs for STORM, plasmids encoding N-cadherin-smFP_HA and smFP_V5 were co-*in utero* electroporated into mouse embryos at E16.5. Ultrathin (500 nm) frozen sections were immunolabeled with antibodies coupled to the photoswitchable dyes Atto488 and Alexa647 for two-color imaging (**Fig. 6**). smFP_V5 provided a very dense cytoplasmic fill that facilitated super-resolution imaging of fine dendritic spines. N-cadherin-smFP_HA showed strong labeling of spine heads and the dendritic shaft, with much weaker labeling of spine necks. The density of the two labels was sufficient for STORM and allowed the reconstruction of both fine dendritic neuropil and N-cadherin cluster localization within spines.

5.3 Electron microscopy

Electron microscopy provides extremely high-resolution images of biological specimens, and remains the gold standard for unambiguous identification of synapses. The native electron-scattering contrast of most tissues is low, and samples are typically enhanced through the addition of electron-dense agents such as osmium tetroxide (OsO_4)

and uranyl acetate (UA). In addition to providing electron contrast, OsO_4 is a powerful cross-linking fixative, dramatically improving lipid membrane ultrastructure and overall EM image quality. However, proteins are also attacked by OsO_4, and antigenicity is routinely destroyed by EM fixation protocols. As a result, users are forced either to preserve tissue without OsO_4, which sacrifices EM image quality, or to perform pre-embedding immunoEM labeling, which decreases antibody penetration. Given that the smFPs robustly enhance labeling in light microscopy experiments, we tested the efficacy of these probes in cell type-specific tracing of neuronal processes by immunoEM.

smFP_FLAG_bright and smFP_myc were delivered to mouse cortical layer 2/3 pyramidal cells by *in utero* electroporation (**Fig. 7a**). Two weeks later, native fluorescence from smFP_FLAG_bright guided excision of the electroporated region. The tissue was prepared by high-pressure freezing (HPF) and freeze substitution (FS) and embedded in HM20 resin (Dahl and Staehelin 1989) (**Fig. 7a**). Ultra-thin (60 nm) serial sections were cut and stained with primary antibodies and then secondary antibodies coupled to 6nm or 12nm gold particles (for smFP_myc and smFP_FLAG, respectively). After silver enhancement, both probes showed specific labeling of transfected cell bodies and neurites with minimal background (**Fig. 7b,d, Supp. Fig. 11**). The labeling was consistently strong in neurites spanning serial sections, which allowed 3D reconstruction through the block (**Fig. 7c,e, Supp. Figs. 11-14**). Both probes tested here completely fill fine neuronal processes, enabling cell type-specific tracing of long-range connections. This performance also enables targeting of EM labels to genetically defined populations of neurons, their processes and synapses.

We also tested the ability of (one of) the smFP tags to survive strong fixation. The smFP_HA label persisted even in samples fixed with 4% PFA / 0.2% glutaraldehyde / 1% OsO$_4$ (**Fig. 7f**), providing strong gold particle labeling (**Fig. 7g,h**). This enables immunoEM detection of defined cells and proteins in samples with the best possible ultrastructure preservation. The use of additional distinguishable gold particle sizes, or other complementary detection methods, should allow expansion of the number of simultaneously detected proteins and/or traced cell populations.

Supplementary figures for Chapter 3:

Appendix Figure 3.1

Schematic of smFP constructs. a-c) Protein structures of sfGFP, mRuby2 and mWasabi with tag insertion sites**.** Left: sfGFP (Protein Data Bank identifier 2B3P), middle: mRuby2 (based on mRuby: 3U0M), right: mWasabi (based on mTFP1: 3HQK). Blue ball, N-terminus; red ball, C-terminus; yellow balls, insertion site: sfGFP (172-173), mRuby2 (167-168), mWasabi (175-176). **d-h**) Molecular models of peptide epitopes in antigenic context. **d) Myc tag**. PDB 1NKP shows the c-myc epitope in the context of folded Myc-max/Mad-max. The myc epitope is highly helical. Therefore, helix-promoting linkers were used: A linkers used between terminal tags; GGA between smFP and inserted tags; AA between inserted tags; and GGGG between the middle two inserted tags, which must "turn around" before going back into the smFP insertion site. Density for full EQKLISEEDL myc tag shown in this figure. **e) V5 tag**. PDB 2B5L shows V5 epitope in the context of folded simian virus 5 V protein. The epitope forms a "mini-domain" structure. Therefore, longer linkers were used between epitopes to space out antibody-binding sites, but were kept as "neutral" secondary-structure preference. QQQ

linkers are used between terminal tags; GG between smFP and inserted tags; QQQ between inserted tags; and GGQQGG between the middle two inserted tags. Density for full GKPIPNPLLGLDST V5 tag shown in this figure. **f) FLAG tag**. PDB 2G60 shows the crystal structure of anti-FLAG tag antibody M2 (Roosild et al. 2006). Green: heavy chain, blue: light chain. A theoretical model showed the DKYD of the DKYDDDDK epitope to be complementary to the binding cleft presented. Shorter linkers were used: G linkers used between terminal tags; GG between smFP and inserted tags; QQ between inserted tags; and GQQG between the middle two inserted tags. **g) strep II tag.** PDB 1KL3 shows strep II tag in complex with streptavidin. The epitope is highly helical in this structure, and is likely to be helical when bound by antibodies, as well. QGQ linkers used between terminal tags; GS/SG between smFP and inserted tags; GGG between inserted tags; and GGQQGG between the middle two inserted tags. **h) HA tag**. PDB 1HIM shows the HA tag in complex with an IgG antibody. Green: heavy chain, blue: light chain, red: peptide. Electron density for YDVPDYA of the YPYDVPDYA HA tag, with a C-terminal S. Tag shows extended structure.

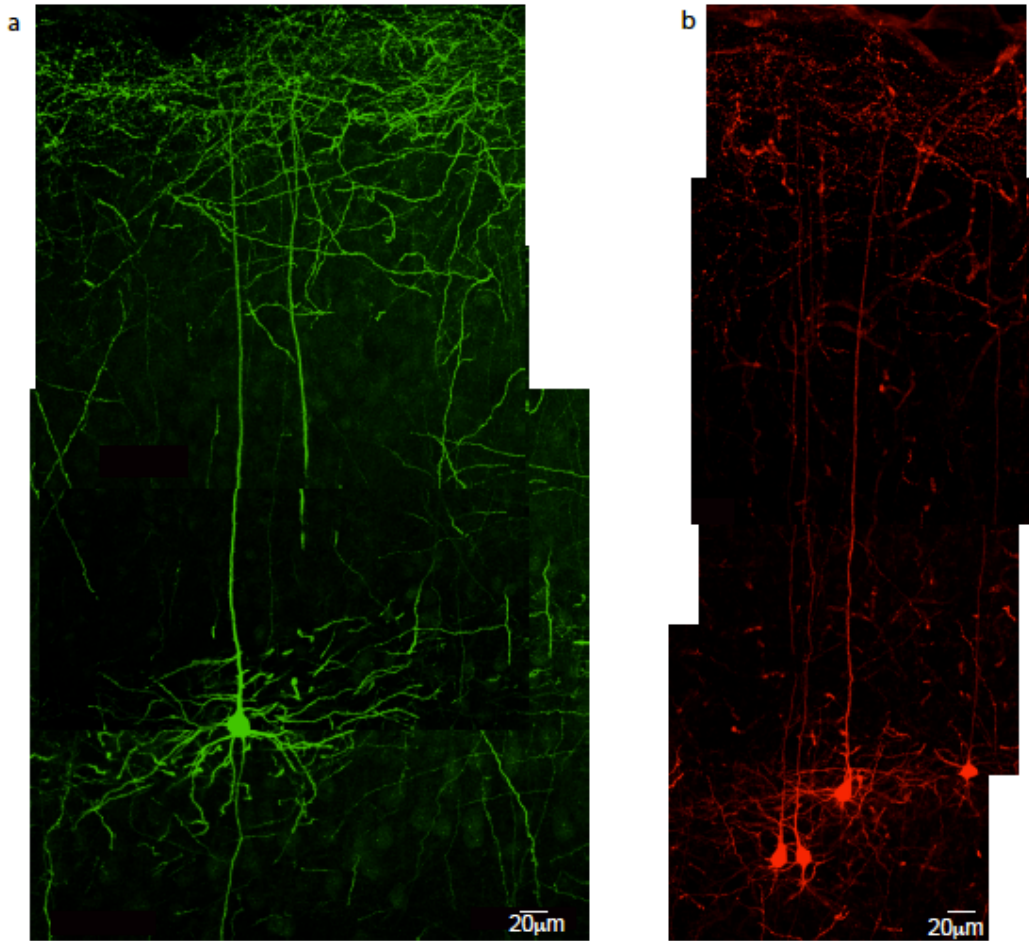
Appendix Figure 3.1
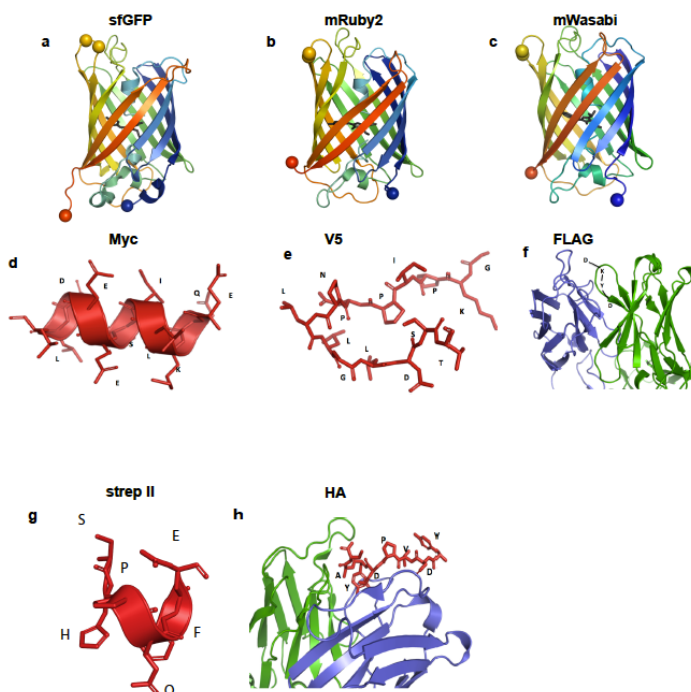
Appendix Figure 3.2
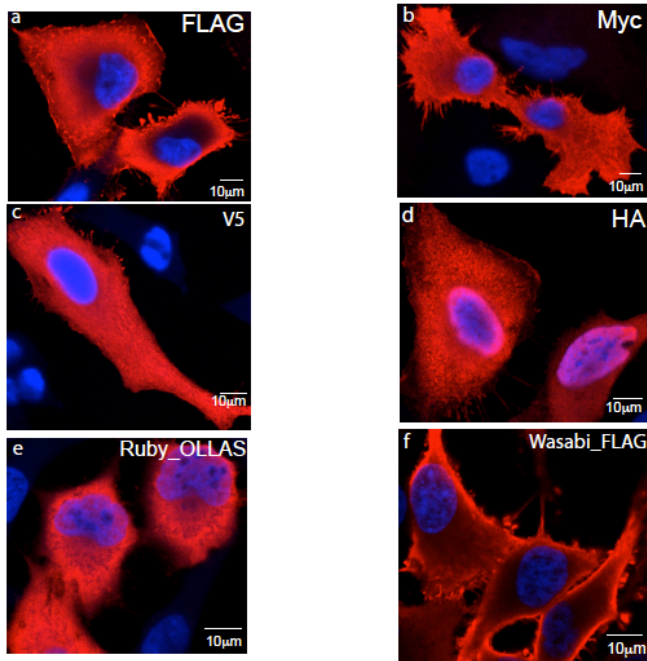
Appendix Figure 2. Expression of smFP constructs in cultured mammalian cells.
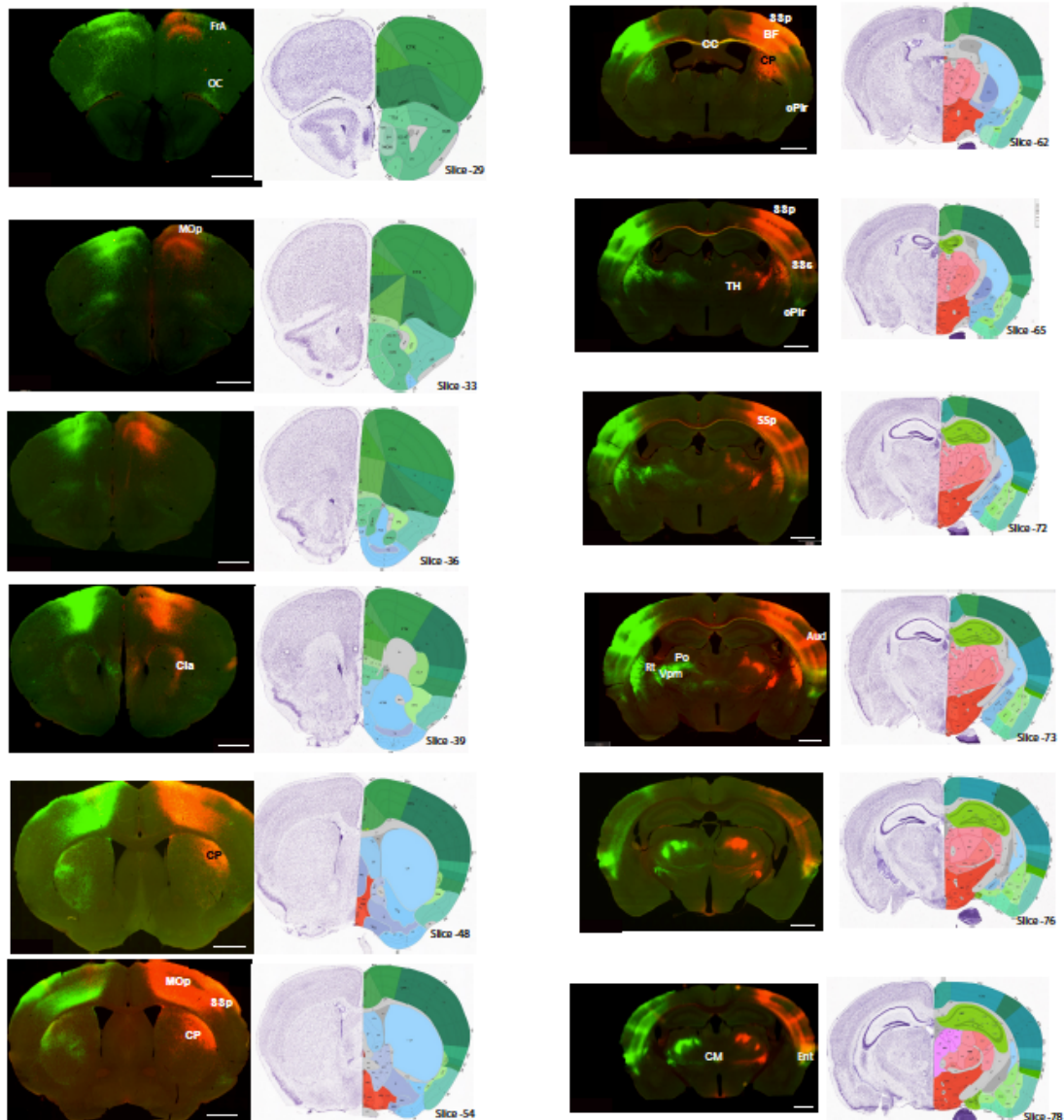HeLa cells were electroporated with plasmids driving cytoplasmic smFP expression from the *CAG* promoter targeting expression to the cytosol and fixed with 2% PFA. smFPs were then detected with primary antibody against the tag and secondary antibody conjugated to Alexa 594. Images were contrast-adjusted in ImageJ. Hoechst stain (blue) shows nuclei. Note the robust expression of smFPs without any obvious sign of cytotoxicity.

Appendix Figure 3.4

Appendix Figure 3.3. Complete filling and labeling in mouse brain slices . a) Layer 2/3 cortical pyramidal neuron in mouse brain slice expressing smFP_myc detected with primary anti-myc antibody and Alexa 488-conjugated secondary antibody. **b)** Layer 5 cortical pyramidal neuron expressing smFP_FLAG detected with primary anti-FLAG antibody and Alexa 594-conjugated secondary antibody. Note complete filling of apical and distal dendrites. Images collected on a Zeiss 510 confocal microscope and contrast-adjusted in ImageJ.

Abbreviations: FrA - Frontal Asociation Cortex. Oc - Orbital Cortex, Cla- Claustrum, CP -Caudoputamen, Mop - Motor area Primary, SSp - Somatosensory Cortex - Primary, SSs - Somatensry Cortex - secondary, CC- corpus callosum, BF - Barrel Field, cPir - contralateral Piriform cortex, TH - thalamus, Rt - Reticular Thalamus, Ent - Entohinal cortex, Aud - Auditory cortex, Po - thalamic nucleus, Vpm - thalamic nucleus, CM - Central Medial nucleus

Appendix Figure 3.4. Projection tracing with smFPs. Fluorescence images of projections following injection of AAV-*CAG*-smFP_myc into left-hemisphere S1 and AAV-*CAG*-smFP_FLAG into right-hemisphere S1. Various coronal slices are shown through the brain highlighting the label density. At right are the corresponding images from the standard reference atlas (http://mouse.brain-map.org/static/atlas). In all images, smFP_myc is stained with primary anti-myc antibody and Alexa 488-conjugated

secondary antibody. smFP_FLAG is stained with primary anti-FLAG antibody and Alexa 594-conjugated secondary antibody. Abbreviations: FrA - Frontal association cortex. Oc - Orbital cortex, Cla- Claustrum, CP -Caudoputamen, Mop - Motor area -primary, SSp - Somatosensory cortex - primary, SSs - Somatosensory cortex - secondary, CC- Corpus callosum, BF - Barrel field, cPir - Contralateral piriform cortex, TH - Thalamus, Rt - Reticular thalamus, Ent - Entorhinal cortex. All images collected on a Perkin-Elmer Pannoramic 250 scanner.
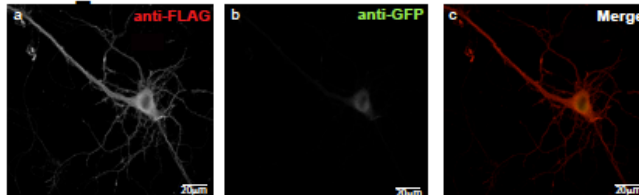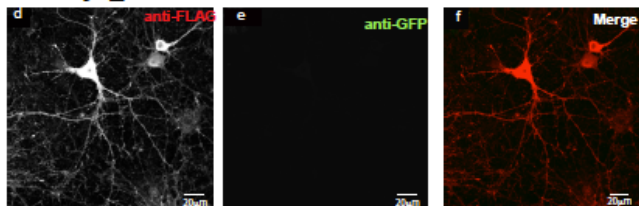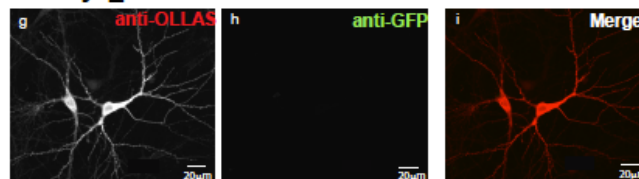
**Appendix Figure 3.5. smFPs based on non-GFP scaffolds do not stain with anti-GFP antibodies. a-c**) Primary hippocampal neurons electroporated with smFP_FLAG. **d-f**) smFP_mRuby_FLAG. **g-i**) smFP_mRuby_OLLAS. Panels a, d and g show neurons detected by antibodies against the respective tag and secondary antibodies conjugated to Alexa 594. Panels b, e and h show neurons stained with anti-GFP antibody and secondary antibody conjugated to Alexa 488. Panels c, f and i show the green and red channels merged. While GFP-based smFPs are detected with anti-GFP antibody, mRuby2-based constructs do not stain.
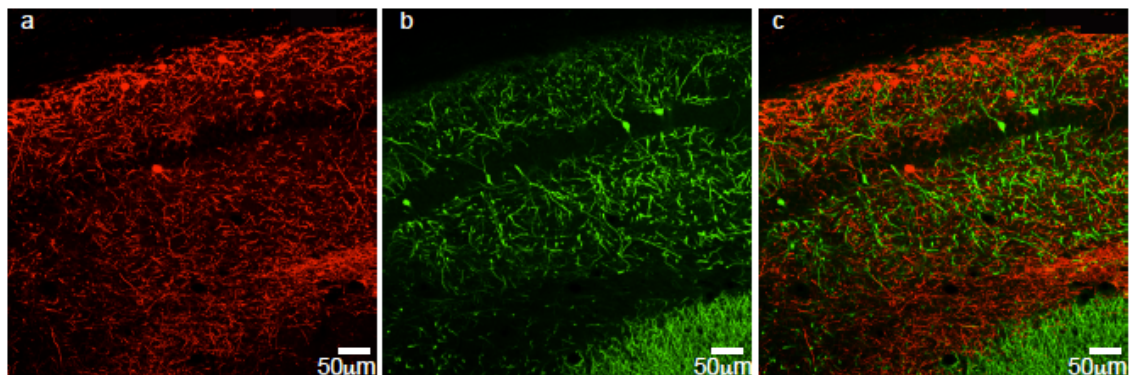
Appendix Figure 3.6 Orthogonality of mRuby2-based smFPs with anti-GFP antibodies in brain slice. *Sst*-Cre * *Thy1*-eGFP double transgenic mouse injected with Cre-dependent AAV-*CAG*-FLEX mRuby2_FLAG virus. mRuby2_FLAG is expressed exclusively in Sst$^+$ interneurons; eGFP from the *Thy1* promoter labels pyramidal neurons. **a-c**) field of view of hippocampus expressing mRuby2_FLAG. Panel a shows neurites detected by anti-FLAG and secondary-Alexa 594, panel b shows neurites detected by

anti-GFP and secondary-Alexa 488, and panel c shows the merge of anti-FLAG and anti-GFP, which show no overlap. Images acquired on a Zeiss 510 confocal microscope and contrast-adjusted in ImageJ.

Appendix: Morphological Diversity of SPN

6.0 Introduction:

The nervous system is primarily composed of complex cellular components called neurons. Although most neurons have the same basic structure – cell body (soma) and processes called axons (output) and dendrites (input), they are highly diverse in nature. Neurons can differ dramatically in their shape/size of soma, and the length, branching and complexity of the processes and overall orientation (Brown, Gillette et al. 2008). Depending on these factors, neurons are classified into different "shapes" or morphological subclasses.

The morphology of a neuron is indicative of its role in connectivity (Cajal 1899). Extensive axonal and dendritic arbors of a neuron play important roles in wiring the neuron with its pre- and post-synaptic partners. Hence the cellular architecture of neurons is an important determinant of their synaptic connectivity. Some critical determinants of

morphology include the shape and arrangement of processes – axons (Catalano,

Robertson et al. 1996) and dendrites (Koch 2012), shape and size of the cell body

(Oyster, Takahashi et al. 1982, Mason and Larkman 1990), extent of dendritic and axonal

branching (Ferrante, Migliore et al. 2013), and the presence of specialized dendritic post-

synaptic structures called spines (Yuste and Denk 1995) (Figure 6.1a).

a)

Oblique dendrite

Spines

Apical dendrite

Soma

Basal dendrite   Axon

b)

Soma

Dendrites

Axon

c)

Bifurcation

Apical dendrite

Bifurcating apical dendrite

Soma
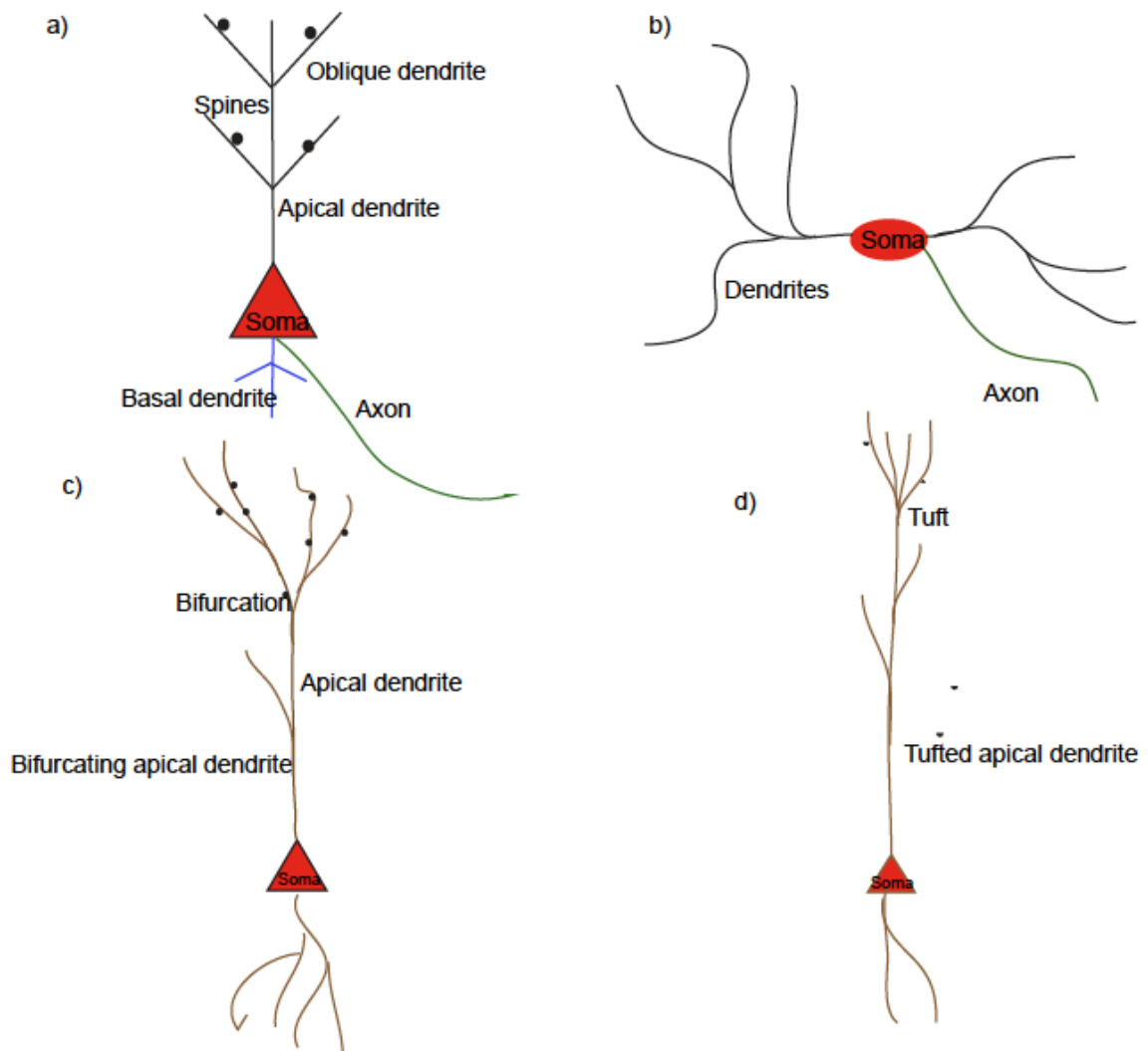
d)

Tuft

Tufted apical dendrite

Soma

Figure 2.1 : General structure of a neuron
Panel a shows the structure of a pyramidal neuron showing the cell body (soma) in red
apical dendrite black with oblique branches and spines, basal dendrite (blue) and axon(green)

Panel b shows the general scheme of an atypical neuron. the dendrites donot seggregate into
basal or apical dendrites. .

Panel c and d show the different types of pyramidal neurons. Panel c shows a pyramidal neuron
bifurcating apical dendrite. Panel d shows a pyramidal neuron with tufted apical dendrite

The role of morphology extends beyond connectivity. Neuronal structure and morphology can be used to predict the function of neurons and circuits, and is valuable as input to computational simulations (Chklovskii 2004, Markram 2006). Hence a systematic morphological characterization of neuronal morphology is a valuable dataset for the study of structure/function and connectivity of neuronal populations. The importance of morphological data in neuroscience is highlighted by the efforts put into the development of automated algorithms to perform 3D reconstruction of neuronal morphologies - (*e.g.* DIADEM - Digital Reconstruction of Axonal And Dendritic Morphologies challenge) and the large-scale curation of such data sets (*e.g.* Neuromorpho.org).

SPN are morphologically heterogeneous (Allendoerfer and Shatz 1994, Kanold and Luhmann 2010, Hoerder-Suabedissen and Molnar 2012). Based on their somato-dendritic morphologies, they have been grouped into distinct classes (Hanganu, Kilb et al. 2002, Kanold and Luhmann 2010). The morphological complexity of SPN was documented in some of the earliest studies in cats (Wahle, Lubke et al. 1994) and mice (Super, Soriano et al. 1998). In more recent years, some studies have attempted a systematic characterization of SP morphologies (Hanganu, Kilb et al. 2002, Hoerder-Suabedissen and Molnar 2012).

Hanganu *et al.* studied ~178 SPN neurons in rats and classified them into six morphological types – horizontal bitufted, monotufted, multipolar, inverted pyramid, tripod and vertical (Hanganu, Kilb et al. 2002). However the authors did not attempt to tackle functional differences between the classes. A more recent study tried to

characterize the morphology of SPN projecting to specific targets (Hoerder-Suabedissen and Molnar 2012).

While all these studies tried to correlate morphology with intrinsic physiological properties and projection targets, the correlation between morphology and molecular identity remains poorly understood. Inhibitory neurons in the neocortex exhibit a correlation between molecular profile and neuronal geometry (Markram 2006, Druga 2009). Since SPN express a range of molecular markers (Allendoerfer and Shatz 1994, Hoerder-Suabedissen, Wang et al. 2009, Kanold and Luhmann 2010), we tried to investigate the neuronal architecture of a particular molecular subclass of SPN.

6.1 Specific Aim:

The goal of this study is to see if SPN can be grouped into distinct morphological classes, and if possible to correlate this with molecular expression patterns.

6.2 Morphological characterization of CTGF positive SPN:

CTGF (Connective Tissue Growth Factor): This gene is expressed in a SP-specific manner within the cortical plate (Heuer, Christ et al. 2003). CTGF gene expression within the SP has an embryonic onset of expression and the gene expression level undergoes post-natal upregulation. While CTGF is expressed in the superplate of *Reeler* mutant mice, it is expressed both in the superficial and deep SP in wild-type mice (Figure 2.6). Since SPN are involved in axon guidance (McConnell, Ghosh et al. 1994), expression of CTGF may have functional significance.

Transgenic lines, which express a specific reporter gene, are indispensible for anatomical and functional studies of the nervous system. We used a bacterial artificial chromosome (BAC) transgenic line expressing GFP from a *CTGF* promoter (Tg(*CTGF*-EGFP)156Gsat) to selectively label SPN and study this particular molecular subclass of SPN.

6.3 GFP expression in the transgenic line:

The Tg(*CTGF*-EGFP)156Gsat line replicates the endogenous gene expression in a very sparse manner. In the neocortex, EGFP expression is confined to the SP zone, but the expression is selective to a subpopulation of the SPN. The expression pattern is described in detail in Chapter 2. This sparseness enabled us to study the morphology of individual SPN and characterize the CTGF positive subpopulation. The goal of this study is to perform a qualitative classification of the neuronal geometry of CTGF positive SPN.

6.4 Results:

6.4.1 CTGF positive SPN belong to a range of morphological subtypes:

In order to observe the morphology of the neurons, we converted the GFP fluorescence to electron density through immunohistochemistry using horseradish peroxidase (HRP) and DAB (3,3-diaminobenzidine), and then reconstructed the neuronal geometry in Neurolucida. This process, on the one hand, eliminated the possibility of photobleaching during reconstruction and also amplified the GFP signal to enable the visualization of fine structures. In addition to this HRP amplification step, we also

observed the native GFP fluorescence using confocal microscopy to visually inspect the neurons.

Fluorescence microscopy and 3D reconstruction of GFP positive neurons in brain slices of the *CTGF*-GFP line revealed three different morphologies:

a) Pyramidal

b) Horizontal

c) Atypical.

6.4.2 Detailed description of the different subclasses with reference to the CTGF positive SPN:

Pyramidal subclass: Pyramidal neurons form the principal neurons in the neocortex (Spruston 2008). Although they are a heterogeneous class of neurons (DeFelipe and Farinas 1992), they can be classified based on some common morphological properties, including (DeFelipe and Farinas 1992):

1. Triangular to ovoid soma

2. Prominent apical dendrites arising from the upper pole radiating towards the *pia mater*. The apical dendrite gives rise to a number of oblique branches

3. From the base arises a set of dendrites directed downwards and in lateral directions. A recent study characterized the morphology of SPN with respect to their projection target and classified pyramidal neurons as "Cells with an identifiable primary dendrite (that was considerably longer than the basal dendrites, and thicker in the initial segment) and often a pyramidal-shaped soma" (Hoerder-Suabedissen and Molnar 2012). Based on these criteria, in this study, we classified neurons as pyramidal if they:

a) Had a pyramidal to oval soma

b) Had a single dendrite that radiated to the *pia* and was longer than the other processes

c) Did not have radial symmetry around the soma.

CTGF positive GFP expressing neurons in this subclass had triangular somata with bases directed towards the white matter and tip facing the *pia*. Although we did not capture the entire length of the apical dendrites, we clearly observed a single apical trunk, originating from the tip of the soma, directed towards the cortical plate. (Figure 6.2) In this transgenic line, the pyramidal subclass represented a minor population of GFP positive neurons (4 out of 21, table 6.1). For some reason, we observed this type more often in preparations used for confocal microscopy.
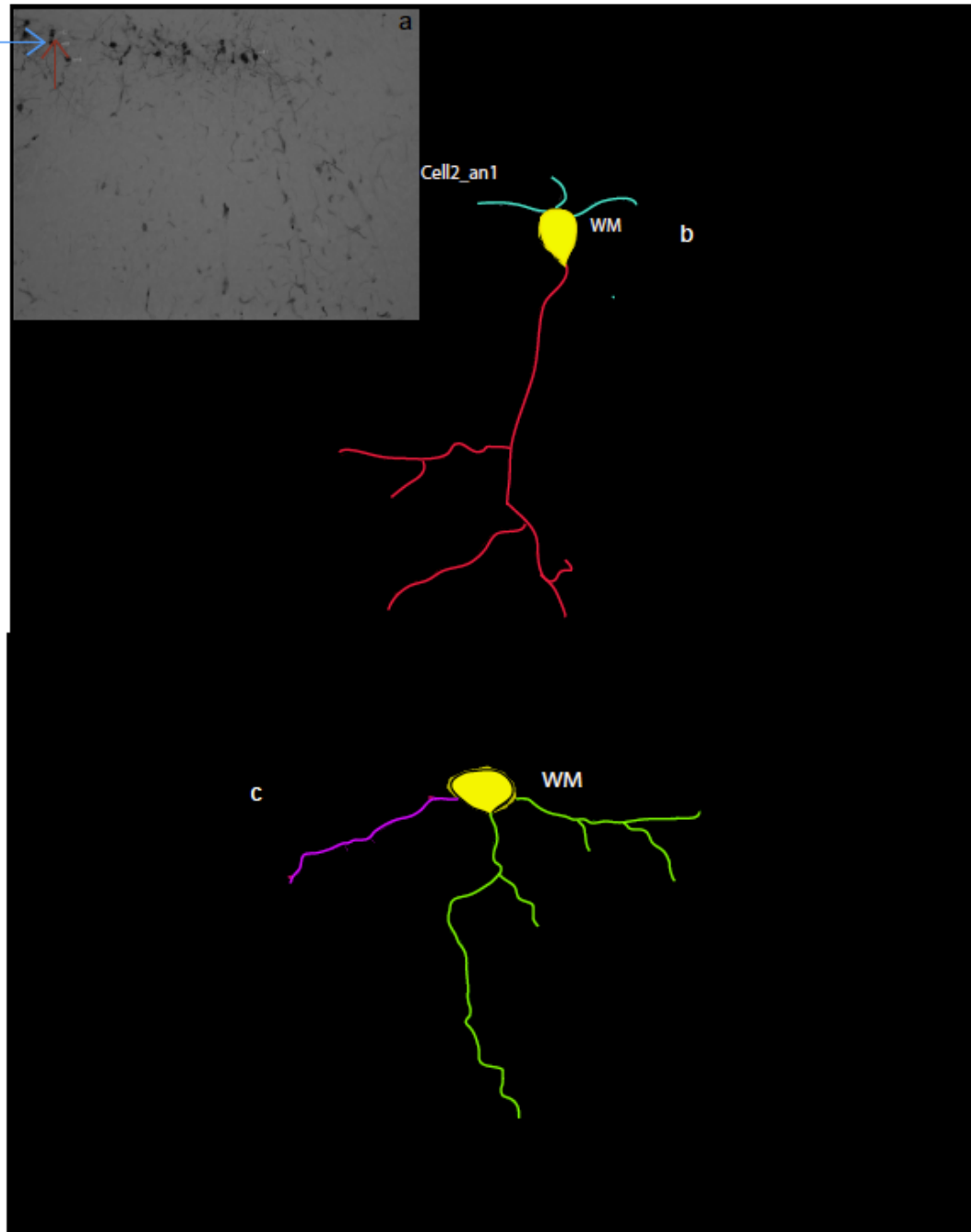
Figure 1.2: CTGF positive Spn that are pyramidal in shape:Figure shows the 3D reconstructions of two CTGF positive Spn, at P7 that are pyramidal in shape. Note the soma shape and distinct dendrites – apical and basal- from these neurons. Inset shows a low power image of the coronal section from P7 mice. CTGF positive SPn are rendered electron dense (black). Arrowheads point to the laminar location of the neurons reconstructed. Red (top) neuron and blue (bottom). Also note the obvious truncation of reconstruction in these neurons.

b) Horizontal subclass: The neurons grouped under this subclass did not have a

prominent apical or basal dendrite and had both their somata and principal processes

oriented parallel to the white matter. We observed this class both in our fluorescent and DAB-stained preparations. The truncated reconstructions precluded further classification of this subtype. However, we did observe differences in the shape and orientation of somata within this subclass. Some neurons in this class had a rounded cell body while others had a triangular soma. Hence there might be distinct subclasses within this group based on the shape of the somata (Figure 6.3). In our preparations (4/19) neurons belonged to this subtype.
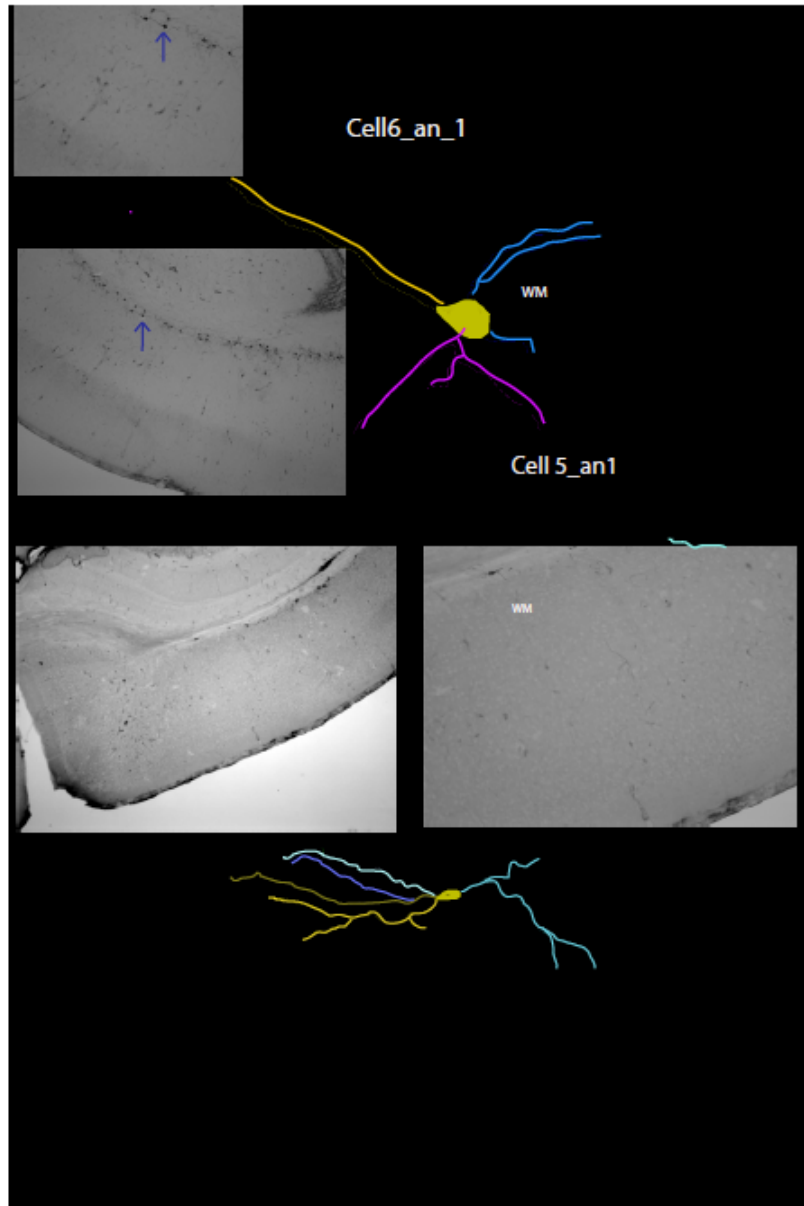
Figure 1.3: CTGF positive Spn that are horizontal in shape: Figure shows the 3D reconstructions of two CTGF positive Spn, at P7 that are horizontal in shape. Insets a and b show a low power image of the a coronal section of a P7 mouse showing the laminar location of the neuron in panel c. Note the laterally extending dendrite and neurites extending into the white matter.Insets a and b show a low power image of the neuron in panel f . Both the reconstructed 3D image and low power image in panel f show neurites entering the WM.

c) Multipolar subclass: Similar to the horizontal subclass, neurons in this category did not posses distinct apical and / or basal dendrites. However they differed from the horizontal subclass in that they were "tilted" with respect to the white matter (Figure 6.4); both the somata and processes appear to be oriented at a particular angle with respect to the white matter. Further criteria are summarized in Table 2.1. The plurality of CTGF-positive SPN belonged to this subclass (7/21). As with the horizontal SPN, a subpopulation in this class had triangular somata while the rest had more rounded somata. Thus depending on the shape of the somata, this subclass could be further subdivided (Figure 6.4 a, b, c,)
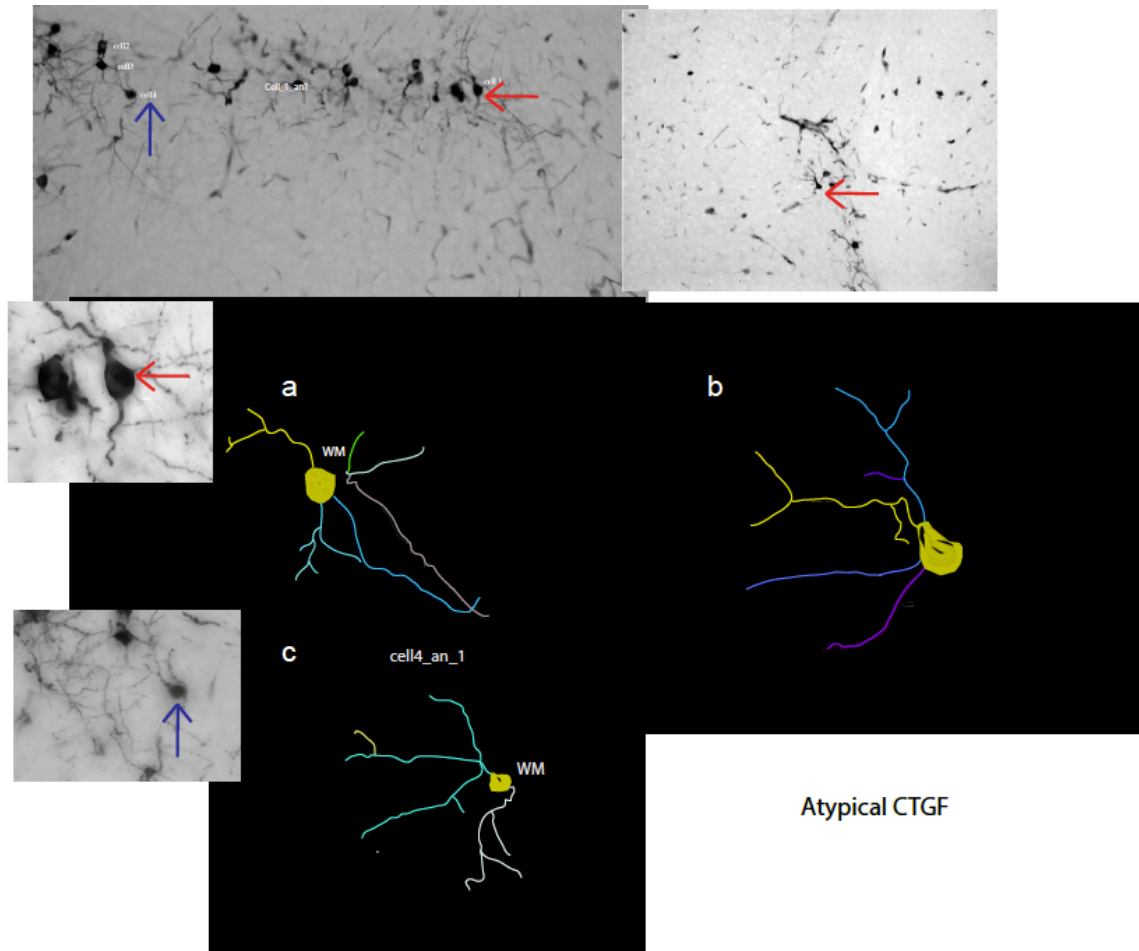
Figure 1.4: CTGF positive Spn that are multipolar in shape: Panel a shows the low power image of the slice showing the laminar location of cells shown in panel c. red arrowhead points to the cell in panel b and c and blue arrowhead points to the cells in panels d and e. Note that the neurites are extended into the WM, CP and also laterally into the SP. Panel d shows neuron in the blue arrowhead in panel a. The 3 d rendering of this neuron is shown in panel e. While the neurite pattern is similar to the one in panel c, note the difference in soma shape and orientation. Panel f shows the low power image of a neuron that is reconstructed in panel g. The soma and the neurite orientation is further different in this neuron. Neurites are seen mostly extending into the CP, and laterally into the SP in one direction.

d) Inverted Pyramid: Very rarely, we observed GFP positive neurons that were pyramidal but the tip was pointed towards the white matter or internal capsule. This subclass was seen only in DAB stained preparations and not in fluorescent preparations. Since DAB staining, being an enzymatic step, allows several fold amplification of the signal , it is likely that these neurons express very low levels of GFP. This subclass is very rare (1 out of 21 neurons). It is interesting that some earlier studies have observed this subclass in interstitial cells (Valverde and Facal-Valverde 1988) (Figure 6.5c).
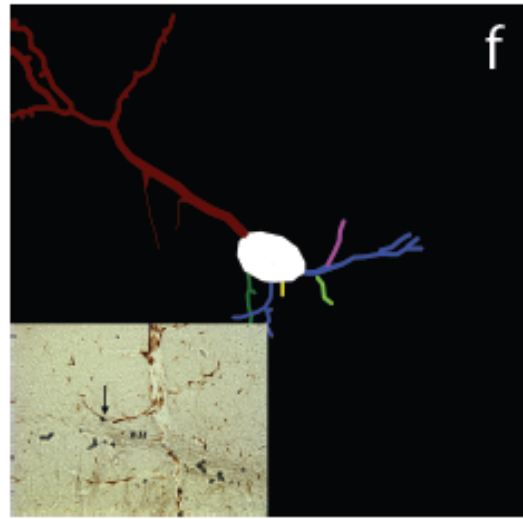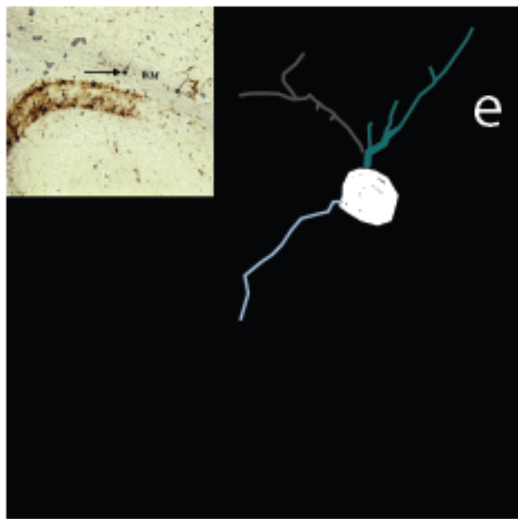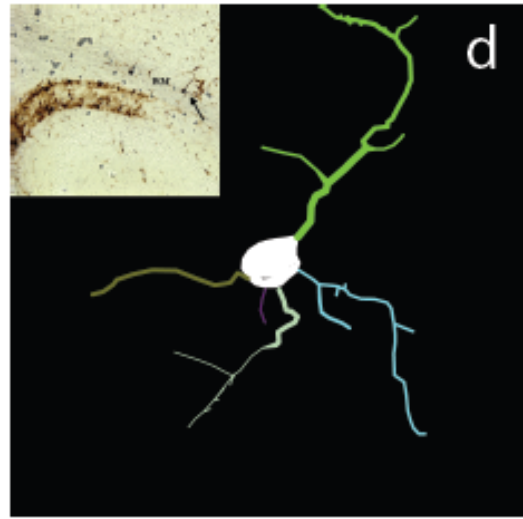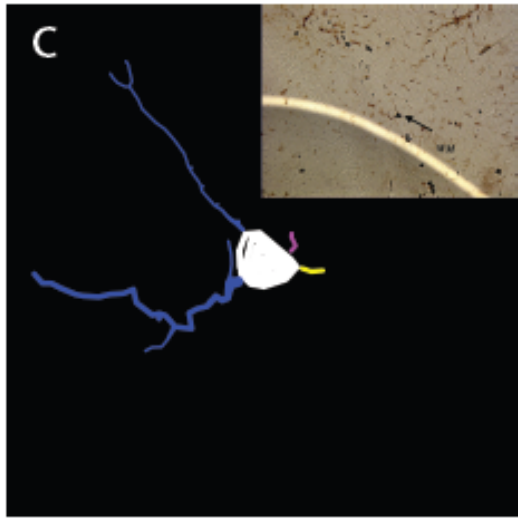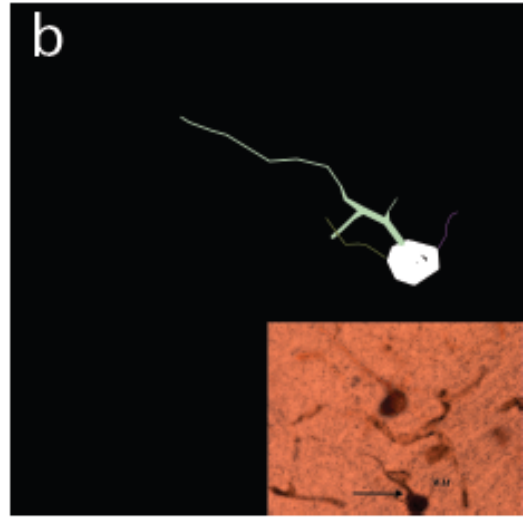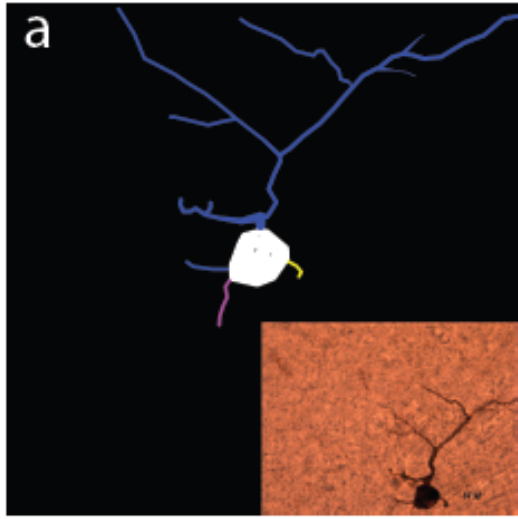
There were also a few neurons (4/21) that, by visual inspection, fell in between the horizontal and atypical classes.

Table 6.1 Criteria for classification: The general criteria for classification are summarized in this table.

Class	Criteria for Classification	Number of cells
Pyramidal	Pyramidal to oval soma A single dendrite that radiated to the pia and was longer than the other processes. Did not have a radial symmetry around the soma	3/19
Horizontal	Both soma and processes are oriented parallel to the WM	6/19
Atypical/Multipolar	Soma and processes are tilted at different angles with respect to the WM Absence of a prominent apical dendrite Processes of almost equal length Radial symmetry of dendrites about the soma	5/19
Atypical/Multipolar (M_t)	Triangular soma	
Atypical (M_r)	Rounded soma	
Multipolar/Horizontal		4/19
Inverted pyramidal	Triangular some with tip facing WM.	1/19

Table 6.2

Summary of characteristics:

The general characteristics of each of the subtypes, soma parameters and distribution of

the processes are summarized in this table.

Cell ID	Shape	Soma	Orientation	Neurites in WM	Spiny	Neurite orientation
1	M	tear-dropshaped at an angle	Horizontal at angle	Yes	Yes	Mostly within lamina
2	P	triangle	Typical pyr		Ns	apical dendrite into CP and basal dendrite into SP
3	P	Triangle but rounded than # 2	Typical pyr			apical dendrite into CP and basal dendrite into SP
4	H/M	Tear drop shaped	Horizontal	Yes	Maybe	Hor. With dense local denritic arbors
5	H	Oval	Horizontal	Yes very prominent	Yes	horizontal and WM projecting
6	H	Tear drop shaped	Horizontal	Maybe		horizontal maybe a truncated upward projecting
7	H	Almost rounded	Horizontal	Yes	Yes	horizontal and WM projecting
8	H	Pyramidal	Horizontal	Yes	Yes	horizontal maybe a truncated upward projecting
9	M	Pyramidal	Horizontal	NS	Yes	mostly local hor
10	H	Pyramidal	Horizontal	Yes	NS	horizontal maybe an upward projecting
11	H	Oval	Horizontal	Ns	Ns	dense within SP and upward projecting
12	M	Triangle	Tip facing upwards	Yes	Yes	horizontal projection within SP.
13	M/H	Tear drop shaped but horizontal	Horizontal	NS	NS	pyramidal but truncated processes
14	P	Triangle	Tip facing upwards Embedded in WM	Ns	Ns	horizontal maybe a truncated upward

						projecting
15	M	Triangle to rounded	Rounded no clear orientation			truncated processes but horizontal and WM
16	IP	Triangle	Tip towards WM		Yes	h proceeses within SP and WM
17	M	Pyramidal	Triangle but horizontal		Yes	h proceeses within SP
18	H/M	Rounded	Rounded no clear orientation		Yes	processes in SP and upward rojecting
19	H/M	Rounded to oval	No clear orinetation		Yes	

6.4.3 Discussion of morphological parameters:

6.4.3.1 Soma shape: Soma shape showed remarkable variation. Shapes ranged from triangular to round. Table 6.2 summarizes the shapes of the somata of the 19 neurons reconstructed. However we found no obvious correlation between soma shape and neuron class.

6.4.3.2 Soma orientation: The somata also had different orientations with respect to the white matter and *pia*. They were oriented at different angles and as with the shape, orientation had no obvious correlation with morphological classification.

6.4.3.3 Dendritic appearance: The GFP positive neurons had dendrites that appeared beaded, especially in confocal images. This beaded appearance was seen both within the SP and all over the cortical plate. Beaded SPN have been described before (Hoerder-Suabedissen and Molnar 2012, (Valverde and Facal-Valverde 1988). Saubadeissen *et al.* observed beaded dendrites in SPN projecting to both intra-cortical and sub-cortical targets at post-natal day 7 (P7).

6.4.3.4 Presence of dendritic spines: Most dendrites had spines, indicating their excitatory nature. However, we could not quantitate the spines in our preparations and could also not associate particular sub-classes with the presence or absence of spines.

6.4.3.5 Dendritic orientation: Dendritic processes were oriented at different angles with respect to the white matter and also the cell body. The ideal way to describe dendritic orientation is through Sholl analysis (described later in this section). However, since our reconstructions were obviously truncated, we did not perform this analysis. Instead we carried out a visual inspection of the dendritic orientation and observed that the neurons extended processes all over the subplate zone and into the cortical plate. Processes, especially dendrites, were seen extending into the internal capsule in all the different subtypes.

6.4.3.6 Laminar Location of CTGF positive SPN: In a previous study, we have shown that SPN could functionally be classified into upper and lower SP (Viswanathan) (Chapter 5). Since CTGF-positive SPN localized in the superplate in the *Reelin* mice, it could be localized in the upper SP. But in our preparations, we found GFP positive neurons in both superficial SP and close to the white matter. Figure 2.6 shows SPN positive for CTGF (green) and Neurofilament H (NFH) (red); we saw both superficial (panel a, top neuron) and deep (panels e and f) neurons. This probably means that neurons belonging to a particular molecular class segregates neither into distinct morphological classes nor into specific laminar locations.

6.5 Further examples of SP diversity: Since these neurons were not completely filled, we also analyzed SPN at different ages filled with biocytin during the critical period (P4-P14). The goal was to obtain completely filled neurons in different classes so that we can further characterize the different morphological subtypes and observe differences in dendritic orientations. We obtained neurons that could be classified as Pyramidal, Atypical and Horizontal. The biocytin fill enabled us to better reconstruct the morphology, and we could characterize the different subclasses more extensively.

6.5.1 Pyramidal: Most of the neurons appeared to posses the typical morphology of pyramidal neurons with a single, long apical dendrite with oblique branches appearing at different angles. Some of them possessed dendritic spines.

However they differed based on:

a) <u>Basal dendrite branching</u> – Some neurons had extensive basal dendrites that had a tufted appearance (Figure 6.7 a,c,e), while some clearly bifurcated

b) <u>Apical tuft</u> – In some cases apical dendrites branched into elaborate tufts before terminating (Figure 6.6a_ a,c). In certain cases, they bifurcated in upper cortical layers (Figure 6.6b_ a,c)

c) <u>Soma shape</u> – neurons possessed either triangular or rounded somata.

We did not find any obvious correlation between the soma shape and dendritic morphologies.
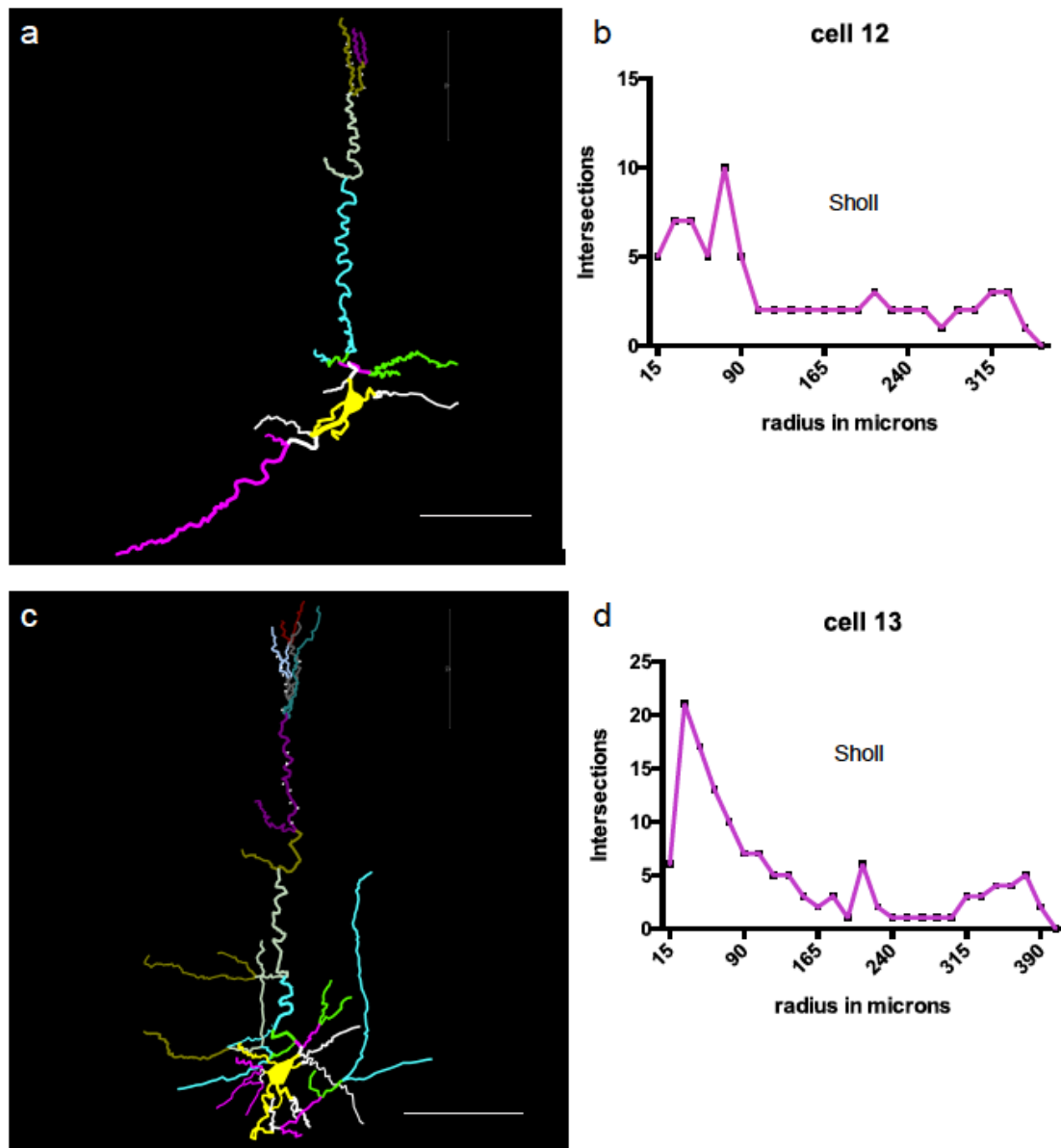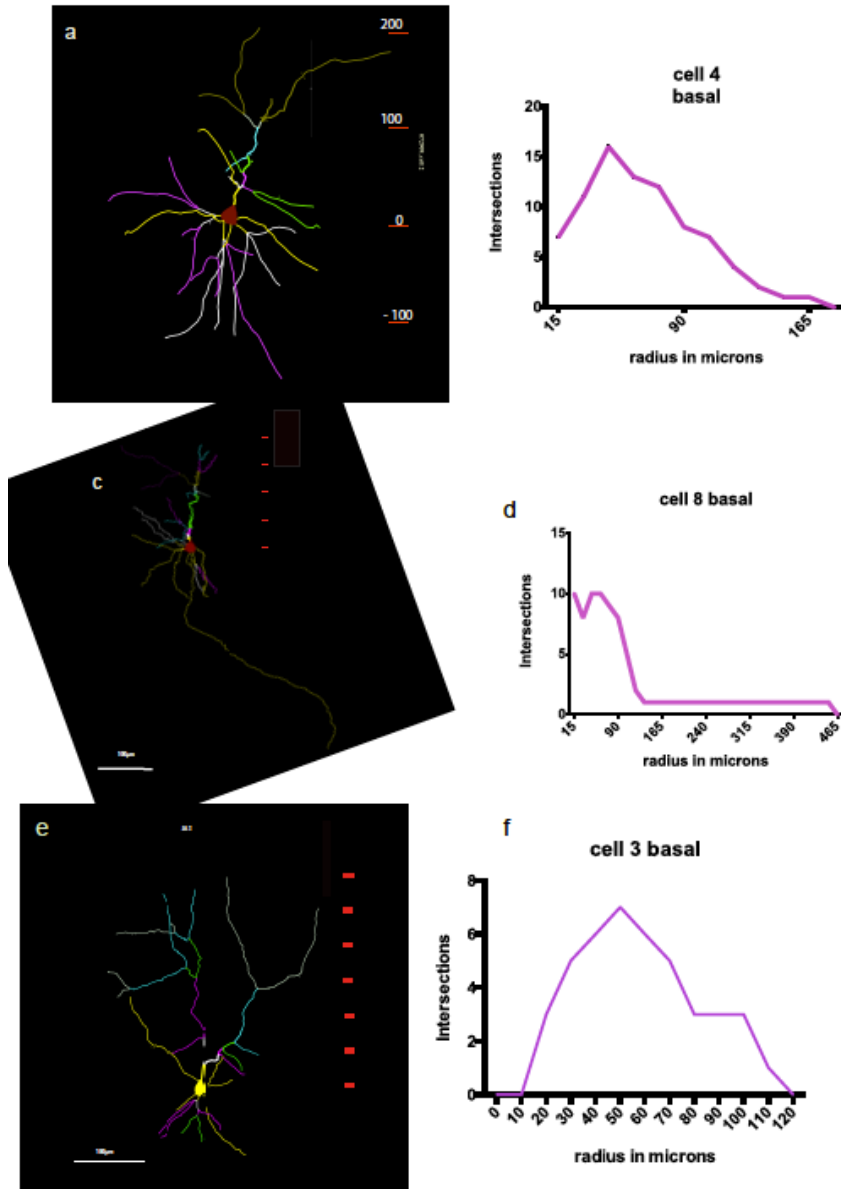
Figure 1.7: Pyramidal neurons with basal dendrites: a) Pyramidal neurons with extensively tufted basal dendrites. The apical dendrite is visibly truncated. b) The sholl diagram of the basal dendrites is shown in panel b. the extensive branching around the soma is reflected in the large number of intersections around the soma. c) Panel c shows another neuron with branched basal dendrites. Note the difference in branching pattern in basal dendrites between the two neurons. d) Sholl diagram for the neuron in panel C . Note the abrupt fall in the number of intersections after a certain distance from the soma. e) Panel e shows a neuron with basal dendrites not as extensively branched as the other examples.

Legend: Types of pyramidal based on basal dendrites : a) Pyramidal neurons with extensively tufted basal dendrites. The apical dendrite is visibly truncted. b) The sholl diagram of the basal dendrites is shown in panel b. the extensive branching around the soma is reflected in the large number of intersections around the soma.

c) Panel c shows another neuron with branched basal dendrites. Note the difference in branching pattern in basal dendrites between the two neurons. d) Sholl diagram for the neuron in panel C . Note the abrupt fall in the number of intersections after a certain distance from the soma. e) Panel e shows a neuron with basal dendrites not as extensively branched as the other examplesf) Sholl diagram for the neuron in panel e. Note the difference in the difference in the number of intersections between the two neurons.

6.5.2 Atypical: These neurons resembled the multipolar class described above, but we chose to call them atypical since in every case, one process was prominent among the others. Neurons were oriented at an angle with respect to the white matter and did not have prominent apical or basal dendrites. Within this class, there was a difference in soma shape and size. Some neurons belonging to this class possessed dendritic spines (Figure 6.8).
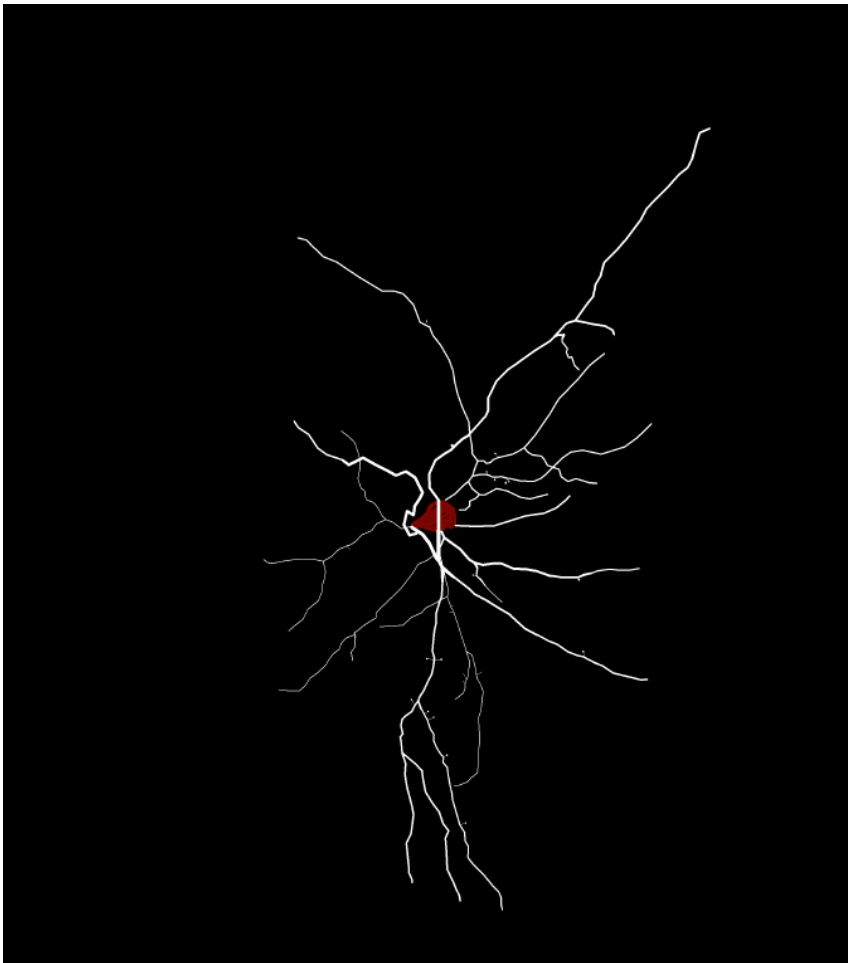
6.5.3 Horizontal: This subclass had somata and principal processes oriented parallel to the white matter. Very few neurons that we recovered belonged to this class and hence we could not characterize this extensively.

6.6 Dendritic branching: We quantitatively analyzed the dendritic morphology by performing Sholl analysis (Sholl 1953). In this method, concentric circles are drawn around the cell body and number of dendritic intersections at each circle is plotted as a function of the radius from the soma (Figure 6.9). This method has been used to reveal the differences in dendritic branching patterns between different subclasses or within each subclass (Mason and Larkman 1990).
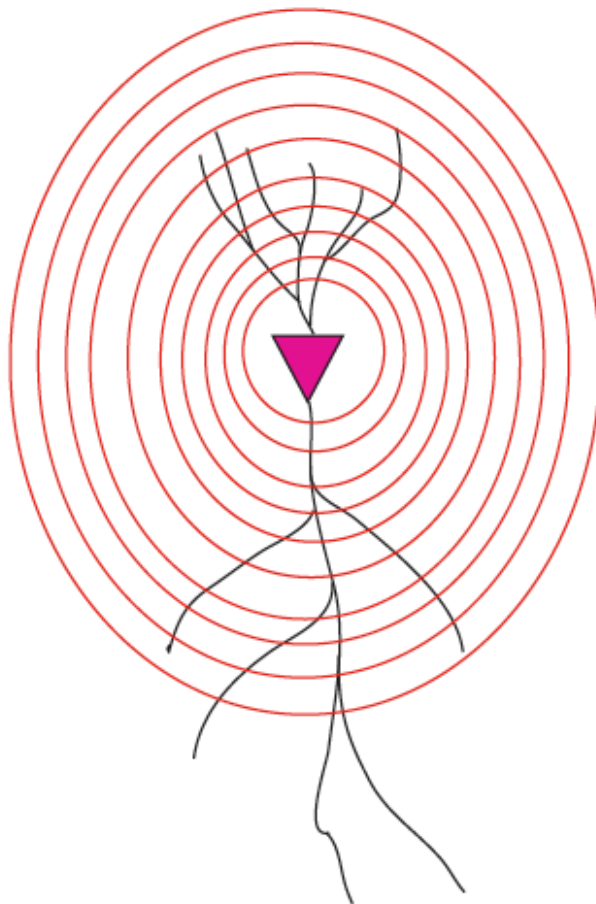
6.6.1 Differences between the different subclasses: Figure 6.10 shows the Sholl plot between pyramidal (magenta) and non-pyramidal (blue) neurons. While pyramidal neurons, on average, extend dendritic branches up to ~400 μm from the soma, non-pyramidal neurons do not branch out beyond 300 μm. Another difference appears to lie within the first 100 μm from the soma. Non-pyramidal neurons branch more extensively within this segment as seen by the increased number of intersections within the first 100 μm.

Sholl analysis of pyramidal neurons VS non pyramidal. X axis shows radius in microns from soma, Y axis shows the number of intersections by dendritic branches. Pyramidal neurons are represented by the magenta bars and non pyramidal ones by the purple bars.
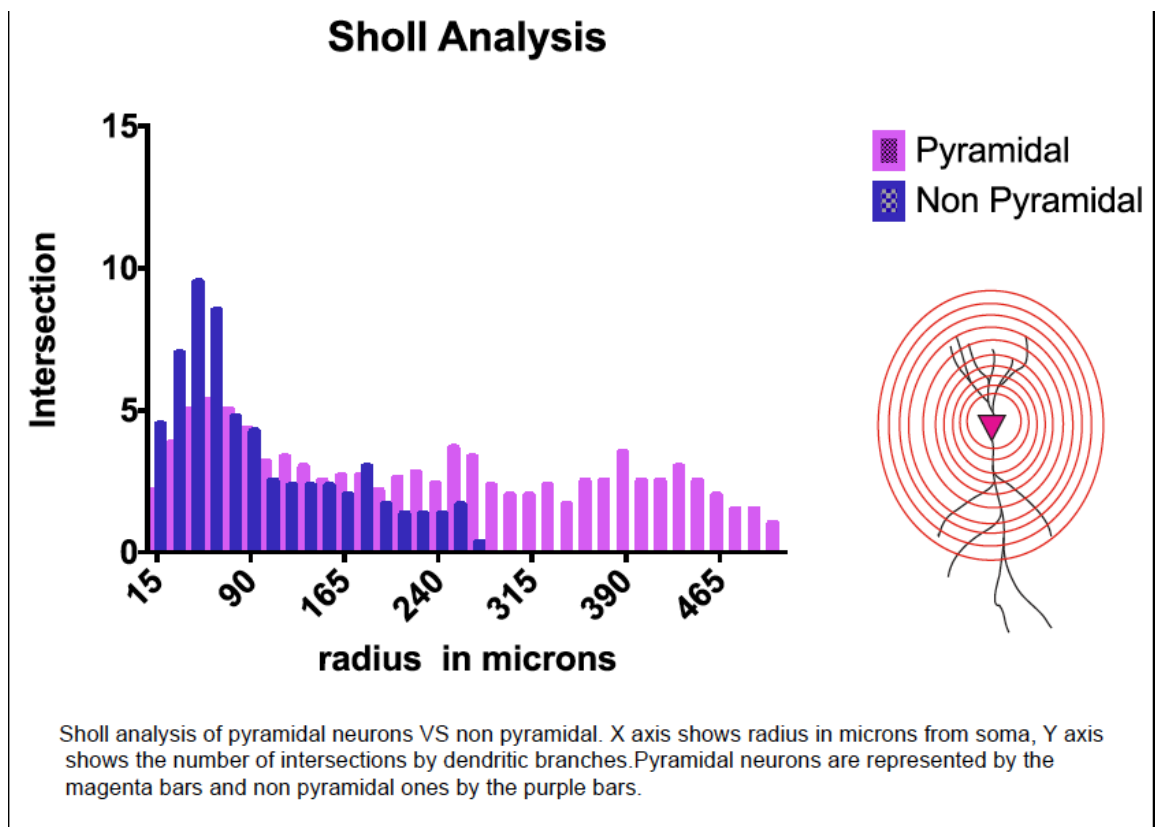
Within the pyramidal subtype, there were some differences beyond 300 μm but some neurons were obviously truncated. So I did not perform comparison within the pyramidal subtype in this dataset. Further datasets with completely filled neurons might reveal differences within individual subtypes.

6.6.2 Dendritic orientation: In order to see if the neurons had a preferred dendritic orientation, we projected the 3D reconstruction as a fan in diagram .We did not find a particular preference for dendritic orientation within a particular class, nor between different classes.

6.7 Discussion:

SPN are integrated into cortical and thalamo-cortical connectivity (McConnell, Ghosh et al. 1994, Kanold, Kara et al. 2003). They are engaged in feed-forward (Zhao, Kao et al. 2009) and feedback (Viswanathan, Bandyopadhyay et al. 2012) connectivity with the CP during the critical period. This population also pioneers thalamo-cortical connections in the embryo (McConnell, Ghosh et al. 1989, McConnell, Ghosh et al. 1994). Hence the same population of neuron is integrated into different aspects of connectivity.

Synaptic connectivity is closely related to neuronal morphology (Chklovskii 2004, Shepherd, Stepanyants et al. 2005, Markram 2006). Hence the precise geometry of the different classes of SPN will be very informative to understand their role in cortical and sub-cortical microcircuitry.

SPN in this study could be grouped into three different morphological classes. Pyramidal neurons are the most abundant class of neurons making up ~70-80% of the neocortex (DeFelipe and Farinas 1992). They are found in almost all mammals (Spruston 2008) and are associated with areas of advanced neuronal functions, such as cortex (Elston 2003) and hippocampus (Schmajuk 1990, Spruston 2008). SPN play a vital role in the establishment of some of the earliest neuronal circuitry in the developing system

and act as an obligate relay of TC circuitry during the critical period. The pyramidal SPN are probably engaged in the neuronal computations required to establish and maintain the "teacher circuit" function.

While the general organizational principles of pyramidal neurons are the same (cartoon), neurons from different species, brain regions, and layers possess differences in structure. One of the common variants between neuronal structures is dendritic morphology, and since the geometry of dendrites affects synaptic integration (Magee 2000, Spruston 2008) this forms an important aspect of structure/function correlation of a neuron.

All the pyramidal neurons we reconstructed had several oblique dendrites along the apical dendrite. We also observed neurons that had thick tufted apical dendrites .These tufted dendrites have also been observed in layer 5 pyramidal neurons (Romand, Wang et al. 2011). It has been shown that inputs from distant targets like TC inputs are received by oblique dendrites and tufts (Petreanu, Mao et al. 2009); for a review see (DeFelipe and Farinas 1992, Bannister 2005, Spruston 2008). Hence it is likely that these neurons are the thalamo-recipient SPN in the relay pathway. Since some CTGF positive neurons are clearly pyramidal, this subclass possibly integrates thalamic inputs into the developing cortical circuitry. It is interesting to note that almost all the pyramidal neurons seen in this study possess dendritic spines.

The dendrites of the atypical neurons extended more locally as compared to the pyramidal neurons (Sholl). Hence they likely serve the local intra-cortical microcircuitry. One of the important findings of this study is that neurons belonging to a particular molecular subclass did not possess a specific neuronal morphology. We observed

different morphological subclasses within the CTGF molecular subclass. It is also likely that CTGF positive SPN are a special subclass that subserve different functions and hence posses different morphologies. Further studies involving reconstruction of other molecular subclasses of SPN could prove if indeed all molecular subtypes of SPN exhibit different geometries.

While the somata presented a range of shapes – round to triangular, the shape did not correlate with any distinct morphological subtype.

A possible caveat of this study is that these neurons were not completely filled. However we carefully chose to study only the properties that were confidently reflected by the reconstructions. We did not study dendritic branch order or quantitate dendritic spines, all of which would have been very informative but incomplete fills could also result in experimental artifacts.

Synaptic connectivity correlates with neuronal morphology (Chklovskii 2004). Hence we made some preliminary attempts to correlate neuronal morphology of SPN with input maps (Laser-scanning photo-stimulation performed by Dr. Linda Meng) and we observed that while pyramidal neurons received columnar inputs from the upper cortical plate, multipolar neurons that extended dendrites locally received local, laminar inputs Further studies correlating morphology with input patterns might reveal a statistically significant correlation between dendritic morphology and connectivity.

Conclusions:

1. Neurons belonging to a particular molecular subclass express diverse morphology.

2. CTGF positive SPN are a diverse population comprising pyramidal, multipolar and horizontal subclasses.

3. Within each subclass, there could be further differences based on soma shape and orientation.

4. The pyramidal subclass of SPN could further be classified based on the presence of apical tufts and the shape of the basal dendrites.

Future directions:

Correlation between dendritic morphologies and synaptic inputs:

We have observed some correlation between dendritic morphology and synaptic inputs to the SPN. Some neurons reconstructed in this study have also been mapped by photolysis of caged glutamate – Laser Scanning Photostimulation (Katz and Dalva 1994) and we observed that neurons that extended axons into the superficial layers received columnar inputs, while those that arborized locally into the CP received local, laminar inputs. Further studies correlating dendritic morphologies with synaptic inputs might be useful in understanding this connectivity.

In this study, we attempted a systematic classification of SPN and showed preliminary evidence for different subclasses within a defined neuronal morphological class. Further studies with intracellular injections with Lucifer Yellow or biocytin, to yield a complete fill, might conclusively prove the existence of the different subclasses of pyramidal neurons.

References _ Appendix chapter 6:

Allendoerfer, K. L. and C. J. Shatz (1994). "The subplate, a transient neocortical structure: its role in the development of connections between thalamus and cortex." Annu Rev Neurosci 17: 185-218.

Bannister, A. P. (2005). "Inter- and intra-laminar connections of pyramidal cells in the neocortex." Neurosci Res 53(2): 95-103.

Brown, K. M., T. A. Gillette and G. A. Ascoli (2008). "Quantifying neuronal size: summing up trees and splitting the branch difference." Semin Cell Dev Biol 19(6): 485-493.

Catalano, S. M., R. T. Robertson and H. P. Killackey (1996). "Individual axon morphology and thalamo-cortical topography in developing rat somatosensory cortex." J Comp Neurol 367(1): 36-53.

Chklovskii, D. B. (2004). "Synaptic connectivity and neuronal morphology: two sides of the same coin." Neuron 43(5): 609-617.

DeFelipe, J. and I. Farinas (1992). "The pyramidal neuron of the cerebral cortex: morphological and chemical characteristics of the synaptic inputs." Prog Neurobiol 39(6): 563-607.

Druga, R. (2009). "Neocortical inhibitory system." Folia Biol (Praha) 55(6): 201-217.

Elston, G. N. (2003). "Cortex, cognition and the cell: new insights into the pyramidal neuron and prefrontal function." Cereb Cortex 13(11): 1124-1138.

Ferrante, M., M. Migliore and G. A. Ascoli (2013). "Functional impact of dendritic branch-point morphology." J Neurosci 33(5): 2156-2165.

Hanganu, I. L., W. Kilb and H. J. Luhmann (2002). "Functional synaptic projections onto subplate neurons in neonatal rat somatosensory cortex." J Neurosci 22(16): 7165-7176.

Heuer, H., S. Christ, S. Friedrichsen, D. Brauer, M. Winckler, K. Bauer and G. Raivich (2003). "Connective tissue growth factor: a novel marker of layer VII neurons in the rat cerebral cortex." Neuroscience 119(1): 43-52.

Hoerder-Suabedissen, A. and Z. Molnar (2012). "Morphology of mouse subplate cells with identified projection targets changes with age." J Comp Neurol 520(1): 174-185.

Hoerder-Suabedissen, A., W. Z. Wang, S. Lee, K. E. Davies, A. M. Goffinet, S. Rakic, J. Parnavelas, K. Reim, M. Nicolic, O. Paulsen and Z. Molnar (2009). "Novel markers reveal subpopulations of subplate neurons in the murine cerebral cortex." Cereb Cortex 19(8): 1738-1750.

Kanold, P. O., P. Kara, R. C. Reid and C. J. Shatz (2003). "Role of subplate neurons in functional maturation of visual cortical columns." Science 301(5632): 521-525.

Kanold, P. O. and H. J. Luhmann (2010). "The subplate and early cortical circuits." Annu Rev Neurosci 33: 23-48.

Katz, L. C. and M. B. Dalva (1994). "Scanning laser photostimulation: a new approach for analyzing brain circuits." J Neurosci Methods 54(2): 205-218.

Koch, C. (2012). "Neuroscience: The connected self." Nature 482(7383): 31-31.

Magee, J. C. (2000). "Dendritic integration of excitatory synaptic input." <u>Nat Rev Neurosci</u> 1(3): 181-190.

Markram, H. (2006). "The blue brain project." <u>Nat Rev Neurosci</u> 7(2): 153-160.

Mason, A. and A. Larkman (1990). "Correlations between morphology and electrophysiology of pyramidal neurons in slices of rat visual cortex. II. Electrophysiology." <u>J Neurosci</u> 10(5): 1415-1428.

McConnell, S. K., A. Ghosh and C. J. Shatz (1989). "Subplate neurons pioneer the first axon pathway from the cerebral cortex." <u>Science</u> 245(4921): 978-982.

McConnell, S. K., A. Ghosh and C. J. Shatz (1994). "Subplate pioneers and the formation of descending connections from cerebral cortex." <u>J Neurosci</u> 14(4): 1892-1907.

Oyster, C. W., E. S. Takahashi and D. C. Hurst (1982). "Analysis of neuronal soma size distributions." <u>J Neurosci Methods</u> 6(4): 311-326.

Petreanu, L., T. Mao, S. M. Sternson and K. Svoboda (2009). "The subcellular organization of neocortical excitatory connections." <u>Nature</u> 457(7233): 1142-1145.

Romand, S., Y. Wang, M. Toledo-Rodriguez and H. Markram (2011). "Morphological development of thick-tufted layer v pyramidal cells in the rat somatosensory cortex." <u>Front Neuroanat</u> 5: 5.

Schmajuk, N. A. (1990). "Role of the hippocampus in temporal and spatial navigation: an adaptive neural network." <u>Behav Brain Res</u> 39(3): 205-229.

Shepherd, G. M., A. Stepanyants, I. Bureau, D. Chklovskii and K. Svoboda (2005). "Geometric and functional organization of cortical circuits." <u>Nat Neurosci</u> 8(6): 782-790.

Sholl, D. A. (1953). "Dendritic organization in the neurons of the visual and motor cortices of the cat." <u>J Anat</u> 87(4): 387-406.

Spruston, N. (2008). "Pyramidal neurons: dendritic structure and synaptic integration." <u>Nat Rev Neurosci</u> 9(3): 206-221.

Super, H., E. Soriano and H. B. Uylings (1998). "The functions of the preplate in development and evolution of the neocortex and hippocampus." <u>Brain Res Brain Res Rev</u> 27(1): 40-64.

Valverde, F. and M. V. Facal-Valverde (1988). "Postnatal development of interstitial (subplate) cells in the white matter of the temporal cortex of kittens: a correlated Golgi and electron microscopic study." <u>J Comp Neurol</u> 269(2): 168-192.

Viswanathan, S., S. Bandyopadhyay, J. P. Kao and P. O. Kanold (2012). "Changing microcircuits in the subplate of the developing cortex." <u>J Neurosci</u> 32(5): 1589-1601.

Wahle, P., J. Lubke and J. R. Naegele (1994). "Inverted pyramidal neurons and interneurons in cat cortical subplate zone are labelled by monoclonal antibody SP1." <u>Eur J Neurosci</u> 6(7): 1167-1178.

Yuste, R. and W. Denk (1995). "Dendritic spines as basic functional units of neuronal integration." <u>Nature</u> 375(6533): 682-684.

Zhao, C., J. P. Kao and P. O. Kanold (2009). "Functional excitatory microcircuits in neonatal cortex connect thalamus and layer 4." <u>J Neurosci</u> 29(49): 15479-15488.